

Single-exciton optical gain in semiconductor nanocrystals

Victor I. Klimov¹, Sergei A. Ivanov¹, Jagjit Nanda¹, Marc Achermann¹, Ilya Bezel¹, John A. McGuire¹ & Andrei Piryatinski¹

Nanocrystal quantum dots have favourable light-emitting properties. They show photoluminescence with high quantum yields, and their emission colours depend on the nanocrystal size—owing to the quantum-confinement effect—and are therefore tunable. However, nanocrystals are difficult to use in optical amplification and lasing. Because of an almost exact balance between absorption and stimulated emission in nanoparticles excited with single electron–hole pairs (excitons), optical gain can only occur in nanocrystals that contain at least two excitons. A complication associated with this multiexcitonic nature of light amplification is fast optical-gain decay induced by non-radiative Auger recombination, a process in which one exciton recombines by transferring its energy to another. Here we demonstrate a practical approach for obtaining optical gain in the single-exciton regime that eliminates the problem of Auger decay. Specifically, we develop core/shell hetero-nanocrystals engineered in such a way as to spatially separate electrons and holes between the core and the shell (type-II heterostructures). The resulting imbalance between negative and positive charges produces a strong local electric field, which induces a giant (~100 meV or greater) transient Stark shift of the absorption spectrum with respect to the luminescence line of singly excited nanocrystals. This effect breaks the exact balance between absorption and stimulated emission, and allows us to demonstrate optical amplification due to single excitons.

Numerous technologies—including optical interconnects in microelectronics, lab-on-a-chip chemo- and bio-analyses, optical telecommunications and information processing—would greatly benefit from flexible, chemically processable optical-gain materials that could be manipulated using simple solution-based techniques. One class of such materials is colloidal semiconductor nanocrystals, also known as nanocrystal quantum dots^{1,2}. These are nanoscale crystal-line particles surrounded by a layer of organic ligand molecules. The dual inorganic–organic nature of these structures provides great flexibility for controlling their physical and chemical properties. For example, using the quantum-confinement effect, the nanocrystal emission energy can be tuned by hundreds of milli-electron volts by simply changing the inorganic-core size³. On the other hand, relatively straightforward surface chemistry can be applied to tune nanocrystal chemical reactivity to facilitate their incorporation into, for example, nanophotonic or nanoplasmonic feedback structures for fabricating micro-lasers of various configurations^{4,5}.

Well-passivated nanocrystals are characterized by near-unity photoluminescence quantum yields. However, despite their high emission efficiencies, there are significant challenges to practical applications of nanocrystals in lasing technologies. Because of the degeneracy of the lowest-energy emitting levels, population inversion in nanocrystals can only be achieved if the average number of electron–hole pairs (excitons) per nanocrystal, $\langle N \rangle$, is greater than 1, which implies that at least some of the nanocrystals in the sample must contain multiexcitons⁶. A significant complication arising from this multiexcitonic nature of optical amplification in nanocrystals is highly efficient non-radiative Auger recombination induced by confinement-enhanced exciton–exciton (X–X) interactions. This process results in fast optical-gain decay characterized by picosecond timescales⁷. Demonstrated approaches to reducing Auger rates include the use of elongated nanocrystals (quantum rods)^{8,9} or

core/shell heteronanocrystals^{10,11} that allow X–X coupling to be decreased without losing the benefits of strong quantum confinement. However, the most radical strategy for solving the problem of Auger decay is the development of methods and/or structures that would allow realization of optical gain in the single-exciton regime, for which Auger recombination is simply inactive.

Here we report a successful practical implementation of one such method that makes use of type-II core/shell heteronanocrystals. These heterostructures are engineered in such a way as to separately confine electrons and holes in the core and the shell, respectively. Spatial separation between negative and positive charges results in a strong local electric field, which leads to effective splitting of the degeneracy of the lowest-energy transition by the Stark effect and displaces the absorbing band in singly excited nanocrystals with respect to the emission line. By significantly reducing absorption losses, this effect allows for optical amplification in the single-exciton regime.

The concept of single-exciton gain

Optical gain corresponds to a light–matter interaction regime for which generation of photons by stimulated emission dominates over photon absorption. As in other lasing media, optical gain in nanocrystals requires population inversion—that is, the situation in which the number of electrons in the excited state is greater than that in the ground state. The lowest-energy emitting transition in nanocrystals of II–VI semiconductors studied here can be described in terms of a two-level system that has two electrons in its ground state. Excitation of a single electron (single exciton) across the energy gap (E_g) in this system does not produce optical gain but rather results in optical transparency, for which stimulated emission by a conduction-band electron is exactly compensated by absorption due to the electron remaining in the valence band (Fig. 1a). Stimulated emission

¹Los Alamos National Laboratory, Los Alamos, New Mexico 87545, USA.

dominates over absorption only if the second electron is also excited across the energy gap, indicating that optical gain requires doubly excited nanocrystals, that is, biexcitons. These considerations imply that population inversion in a nanocrystal ensemble can only be achieved if $\langle N \rangle$ is greater than 1.

The condition for optical gain however changes if one accounts for a local electric field associated with an excited electron-hole pair. This field can alter the absorption energy of the electron remaining in the valence band by the carrier-induced Stark effect (Fig. 1b)^{12,13}. If the magnitude of the Stark shift (Δ_S) is comparable to or greater than the transition line width (Γ), it can completely eliminate absorption losses at the emission wavelength in excited nanocrystals, which should allow optical gain using single-exciton states. Specifically, the threshold for population inversion in the presence of the transient transition shift is determined by the condition $\langle N \rangle = 2 / (3 - \exp(-\Delta_S^2 / \Gamma^2))$ (see Supplementary Information). If $\Delta_S \ll \Gamma$, it reduces to $\langle N \rangle = 1$, which corresponds to the usual case of multiexciton optical gain. However, if $\Delta_S \gg \Gamma$, $\langle N \rangle = 2/3$ (Fig. 1c), which implies that optical gain does not require multiexcitons.

Engineered exciton-exciton interactions

The carrier-induced Stark effect can be described in terms of the Coulomb interaction of the initially generated exciton with the exciton created in the second excitation act. In this description, the transient Stark shift is determined by the X-X Coulomb interaction energy ($\Delta_{XX} = \Delta_S$) defined as $\Delta_{XX} = E_{XX} - 2E_X$, where E_X and E_{XX} are single- and biexciton energies, respectively. The X-X interaction

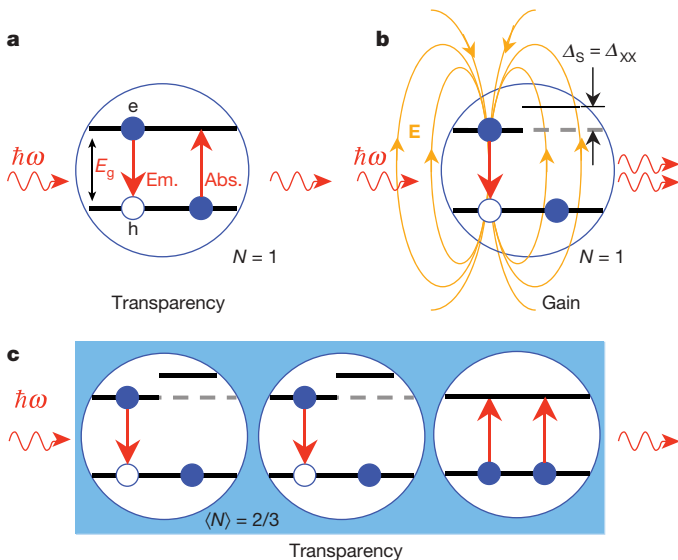


Figure 1 | The concept of single-exciton nanocrystal lasing. **a**, In the absence of X-X interactions, excitation of a single electron-hole pair (single exciton) per nanocrystal (NC) on average does not produce optical gain but results in optical transparency—that is, the regime for which stimulated emission (Em.) is exactly compensated by absorption (Abs.). **e**, Electron; **h**, hole. **b**, The balance between stimulated emission and absorption is broken if one accounts for X-X interactions that spectrally displace the absorbing transition with respect to the emission band. The latter effect can be interpreted in terms of the transition Stark shift ($\Delta_S = \Delta_{XX}$) induced by a local electric field (**E**) associated with a single-exciton state. If the transition shift is greater than the ensemble line width, optical gain can occur in the single-exciton regime. **c**, In the case of large Δ_S ($\Delta_S \gg \Gamma$), stimulated emission in singly excited NCs (n_x is their fraction in the NC ensemble) competes only with absorption in unexcited NCs (fraction $(1 - n_x)$; here, we neglect multiexcitons). The stimulated-emission cross-section of a singly excited NC is one half of the absorption cross-section of the lowest-energy NC transition. Based on these considerations, the optical-gain threshold can be found from the condition $n_x/2 = (1 - n_x)$, which indicates that the single-exciton gain onset corresponds to the situation where two-thirds of the NCs are excited with single excitons.

strength is also often characterized in terms of the biexciton binding energy (δE_{XX}), which relates to Δ_{XX} by $\delta E_{XX} = -\Delta_{XX}$.

The energy Δ_{XX} depends on the local electrical charge density $\rho_X(\mathbf{r})$ associated with a single-exciton state and, hence, on the sum of the hole (ρ_h) and the electron (ρ_e) charge densities: $\rho_X(\mathbf{r}) = \rho_h(\mathbf{r}) + \rho_e(\mathbf{r})$ (\mathbf{r} is the spatial coordinate). Because of almost identical spatial distributions of electron (ψ_e) and hole (ψ_h) wavefunctions, $\rho_X(\mathbf{r})$ is nearly zero in homogeneous nanocrystals ($\rho_X(\mathbf{r}) = e(|\psi_h(\mathbf{r})|^2 - |\psi_e(\mathbf{r})|^2) \approx 0$, e is the electron charge) (Fig. 2a), which leads to relatively small X-X interaction energies of ~ 10 to ~ 30 meV (refs 14, 15). These values are smaller than typical transition line widths in existing nanocrystal samples (ensemble broadening of ~ 100 meV or greater) and, therefore, do not allow significant suppression of absorption at the emission wavelength.

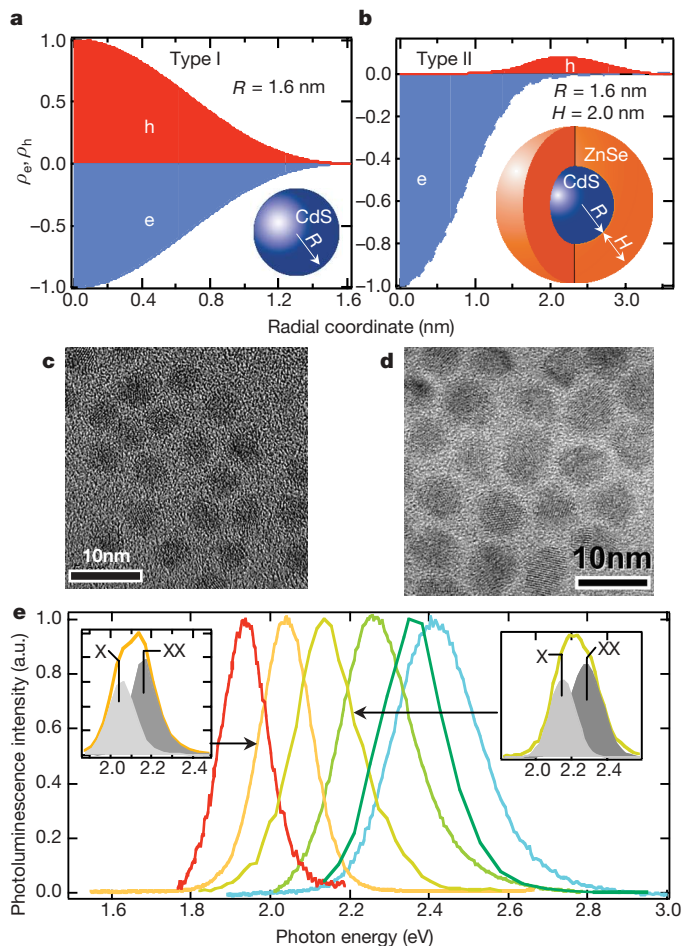


Figure 2 | Type-I CdS NCs and type-II CdS/ZnSe core/shell heterostructures. **a**, Spatial distributions of electron (ρ_e) and hole (ρ_h) charge densities are nearly identical in type-I NCs (inset) (calculated for $R = 1.6$ nm). **b**, In type-II core/shell NCs (inset), electrons are primarily localized in the core, while holes reside in the shell, which leads to a significant difference in radial distributions of ρ_e and ρ_h (calculated for $R = 1.6$ nm and $H = 2.0$ nm). **c**, A transmission electron microscopy (TEM) image of a core CdS particle of ~ 2.4 nm radius. **d**, TEM images of heterostructures fabricated using the cores shown in **c**. The core/shell NC radius is ~ 3.4 nm, indicating that the shell width is ~ 1.0 nm. Because of the small difference between electron scattering cross-sections of CdS and ZnSe, the CdS/ZnSe interface is not discernible in the TEM image. **e**, Emission spectra of a series of CdS/ZnSe core/shell NCs synthesized using CdS cores with radii of 1.6 nm (higher-energy emission) and 2.6 nm (lower-energy emission) and various shell widths. Insets, early-time emission spectra measured at high pump intensities can be deconvolved into the single-exciton (X) and the biexciton (XX) bands. The spacing between these two bands indicates giant X-X interaction energies of more than 100 meV. a.u., arbitrary units.

The separation of electrons and holes between the core and the shell in type-II nanocrystals (Fig. 2b) can lead to sizable local charge densities and, hence, large Coulomb interaction energies¹⁶. To analyse the effect of charge separation on X–X interactions and its influence on optical gain properties of nanocrystals, we study heterostructures composed of a CdS core overcoated with a ZnSe shell (Fig. 2b inset). These nanostructures are synthesized by reacting prefabricated CdS core particles¹⁷ with Zn/Se precursors, which results in CdS(core)/ZnSe(shell) nanocrystals (Figs 2c, d) (details of the synthesis are described in Supplementary Information). As illustrated in Fig. 2e, the emission colour produced by these nanocrystals can be tuned from red to green by varying the core radius and/or the shell thickness.

According to bulk-semiconductor parameters, the bottom of the conduction band is lower in CdS than in ZnSe, while the top of the valence band is higher for ZnSe (Fig. 3a). Therefore, the electron–hole pair generated near the bulk CdS/ZnSe hetero-interface tends to produce a charge-separated state, with the electron residing in CdS and the hole in ZnSe. This situation corresponds to the type-II regime, whereas the regime for which the electrons and the holes co-occupy the same part of a heterostructure is usually referred to

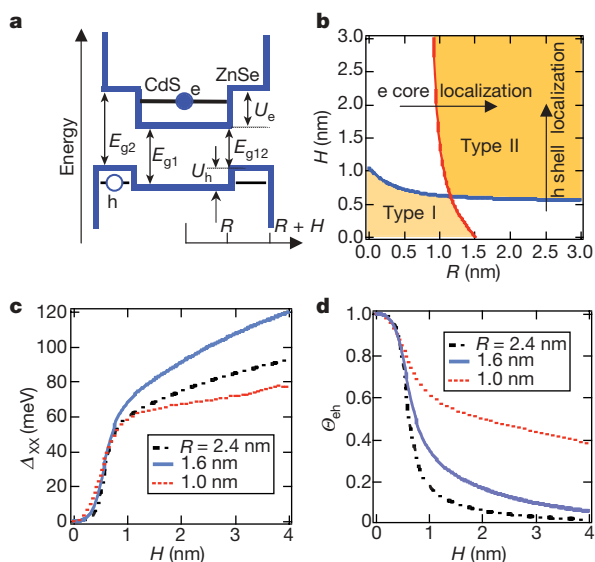


Figure 3 | Electronic structure and different localization regimes in CdS/ZnSe core/shell NCs. **a**, Illustration of alignment of the conduction- and valence-band edges at the bulk CdS/ZnSe interface (blue lines) and the lowest-energy electron and hole quantized levels (black lines) in the CdS(core)/ZnSe(shell) NC. Arrows indicate bulk parameters: $E_{g1} = 2.485$ eV (CdS energy gap), $E_{g2} = 2.72$ eV (ZnSe energy gap), $E_{g12} = 1.925$ eV ('indirect' energy gap of a type-II CdS/ZnSe heterostructure), $U_e = 0.795$ eV (conduction-band energy offset at the hetero-interface) and $U_h = 0.56$ eV (valence-band energy offset at the hetero-interface). **b**, Localization phase diagram that shows the regions of (R, H) -space that correspond to different localization regimes in CdS/ZnSe hetero-NCs. The shaded areas correspond to type-I (both carriers are delocalized over the entire hetero-NC volume) and type-II (electrons and holes are confined to the core and the shell, respectively) regimes. In the unshaded areas, the regime of localization is not well defined; in this case one of the carriers is confined to either the core or the shell, while the other one is delocalized over the entire NC volume. **c**, **d**, The dependence of the X–X interaction energy Δ_{XX} (in **c**) and the electron–hole overlap integral Θ_{eh} (in **d**) on shell width for three core radii of 1.0, 1.6 and 2.4 nm. For all core radii, the increase in Δ_{XX} correlates with the drop in Θ_{eh} , indicating that X–X interactions are enhanced with increasing degree of spatial separation between electrons and holes. From the data for $R = 1.0$ and 1.6 nm, one can see that the more complete spatial separation achievable for 1.6-nm cores produces stronger X–X repulsion. The trend is more complex for larger core sizes (compare data for $R = 1.6$ and 2.4 nm), for which the increase in the interaction energy due to increasing charge imbalance competes with the effect of the decreasing charge density.

as type I. In contrast to a fixed alignment of energy levels at the bulk CdS/ZnSe hetero-interface, the alignment of energy states in CdS/ZnSe nanocrystals depends on the core radius (R) and the shell width (H), which determine the positions of quantized levels with respect to the bulk band edges (see the 'localization' phase diagram in Fig. 3b). Specifically, for small core radii ($R < 1.2$ –1.5 nm) and thin shells ($H < 0.6$ –1.0 nm), these structures yield type-I localization (shaded area in the lower-left corner of Fig. 3b), while the type of localization changes to type II for larger R and H (shaded area in the upper-right corner of Fig. 3b). For the type-I regime, an electron and a hole are delocalized over the entire heteronanostructure and their charge densities nearly cancel each other (Fig. 2a). In the type-II case, electrons reside in the core while holes are in the shell, which leads to a significant difference in the spatial distributions of negative and positive charges and, hence, large local charge densities (Fig. 2b).

A convenient quantity for describing the spatial separation between electrons and holes is the electron–hole overlap integral, $\Theta_{eh} = |\langle \psi_h | \psi_e \rangle|^2$. This quantity also provides a measure of the imbalance between negative and positive charges in the nanocrystal and, therefore, the changes in Θ_{eh} directly correlate with variations in the X–X interaction energy. This effect is illustrated in Fig. 3, which shows Δ_{XX} (Fig. 3c) and Θ_{eh} (Fig. 3d) calculated for CdS/ZnSe nanocrystals for fixed core radii ($R = 1.0, 1.6$ and 2.4 nm) and a varied shell width (details of the calculations are described in Supplementary Information). We observe that the initial increase in H leads to a rapid drop of the overlap integral owing to transition to the type-II regime. The reduction in Θ_{eh} is accompanied by a rapid increase of Δ_{XX} because of an increasing imbalance between positive and negative charges. Specifically, for $R = 1.6$ nm and $H > 2$ nm ($\Theta_{eh} < 0.17$), Δ_{XX} can reach giant values of ~ 100 meV.

It is interesting to examine the sign of the X–X interaction energy. In type-I nanocrystals, Coulomb interactions tend to spatially arrange charges in such a way that the biexciton energy E_{XX} is less than twice the single-exciton energy E_X . This situation corresponds to a negative value of Δ_{XX} (positive biexciton binding energy), which can be interpreted in terms of an effective X–X attraction. In type-II nanocrystals, the spatial distribution of charges is controlled not by Coulomb interactions but by large energy gradients at the core/shell interface, which leads to concentration of the same-sign charges in the same part of the heteronanostructure (both electrons in the core; both holes in the shell) and spatial separation of charges of the opposite sign across the hetero-interface. This type of spatial arrangement increases the repulsive component of the Coulomb interaction and decreases its attractive component, which produces net X–X repulsion¹⁶ (negative biexciton binding energy), as indicated by the positive sign of the calculated values of Δ_{XX} (Fig. 3c). X–X repulsion can also be obtained in type-I nanocrystals if one accounts for the difference between the conduction- and the valence-band structures¹⁸. However, the latter repulsion is significantly smaller than the repulsion discussed in this Article, and so is neglected in our calculations.

The sign of Δ_{XX} has an important effect on the optical-gain properties of nanocrystals because it determines the direction of the shift of the absorbing transitions with respect to the emission line. If Δ_{XX} is negative (X–X attraction), the transitions move downward in energy, which may have a detrimental effect on lasing performance because of increasing absorption due to the manifold of strong transitions located immediately above the emitting band. On the other hand, strong X–X repulsion, which can be produced in type-II nanocrystals, should benefit lasing because it moves strongly absorbing transitions away from the emission line.

Giant exciton–exciton repulsion energies

In order to experimentally measure the X–X interaction energy in type-II core/shell nanocrystals, we compare the position of the biexciton photoluminescence band with respect to the single-exciton line. Radiative recombination of the biexciton produces a photon

($\hbar\omega_{XX}$) and an exciton and hence, $\hbar\omega_{XX} = E_{XX} - E_X = E_X + \Delta_{XX}$. On the basis of this expression, the shift of the biexciton line with respect to the single-exciton band ($\hbar\omega_X = E_X$) provides a direct measure of the X–X interaction energy: $\Delta_{XX} = \hbar\omega_{XX} - \hbar\omega_X$.

The challenge in experimentally detecting photoluminescence from nanocrystal multiexcitons is associated with their short (picoseconds to hundreds of picoseconds) lifetimes, which are limited by non-radiative Auger recombination⁷. Because these times are significantly shorter than the radiative time constants, signals from multiexcitons are not well pronounced in steady-state photoluminescence spectra. Therefore, in order to detect the emission from multiexcitons, we apply time-resolved photoluminescence measurements, in which emission of nanocrystals excited by 200-fs, 3-eV pulses is analysed using time-correlated single-photon counting (~ 30 ps time resolution).

Figure 4a shows photoluminescence spectra of a hexane solution of CdS/ZnSe nanocrystals with $R = 1.6$ nm and $H = 2$ nm recorded at a pump fluence that corresponds to excitation of approximately 1.5 excitons per nanocrystal on average. According to the phase diagram in Fig. 3b, the nanocrystals used in these measurements correspond to the type-II regime, for which electrons and holes are well separated between the core and the shell. The long-time spectrum recorded at time $t = 10$ ns after excitation (filled circles in Fig. 4a) is identical to the steady-state photoluminescence spectrum observed at low excitation fluences ($\langle N \rangle \ll 1$) and corresponds to emission of single excitons ($E_X = 2.054$ eV). The $t = 0$ photoluminescence (open squares in Fig. 4a) indicates the presence of an additional high-energy,

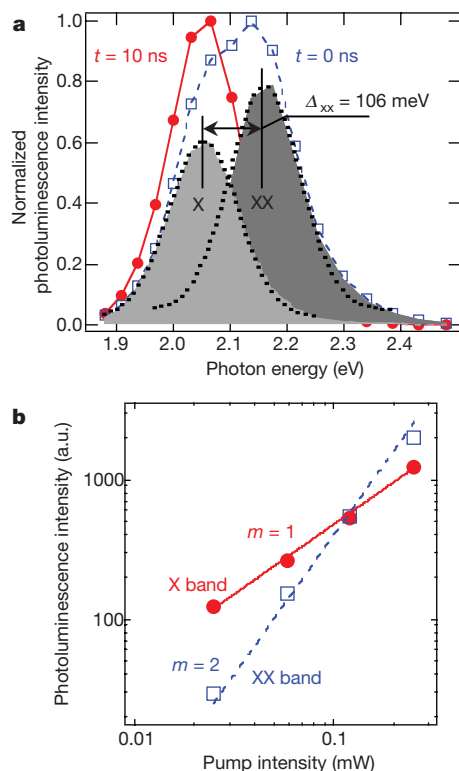


Figure 4 | Experimental demonstration of giant X–X repulsion in type-II CdS/ZnSe NCs. **a**, Short- (open squares) and long- (solid circles) time room-temperature photoluminescence spectra of CdS/ZnSe NCs. Deconvolution of the $t = 0$ spectrum into two bands shown by grey areas (dotted lines are gaussian fits) reveals the short-lived XX feature due to emission from biexcitons that is located to high energies from the single-exciton X band. The spacing between these two bands indicates giant X–X repulsion characterized by $\Delta_{XX} = 106$ meV. **b**, Photoluminescence pump-intensity dependences indicate that the growth of X and XX features with excitation power shows log–log slopes of $m = 1$ and 2, respectively. These slopes are consistent with single-exciton and the biexciton mechanisms for the X and XX emission bands, respectively.

short-lived band at 2.160 eV, which decays with a time constant of ~ 130 ps. This band (feature XX in Fig. 4a) can be extracted from the $t = 0$ spectrum by subtracting an appropriately scaled long-time spectrum (feature X in Fig. 4a).

The measured pump-intensity dependences indicate that the growth of band X is linear in pump fluence (filled circles in Fig. 4b), as expected for single-exciton emission. On the other hand, the high-energy band XX shows a quadratic growth (open squares in Fig. 4b), which is typical for emission from biexcitons. The fast decay of this feature is also consistent with its multiexciton origin, and is due to efficient Auger recombination. Further, this band cannot be attributed to recombination of carriers populating excited nanocrystal states because, according to our transient absorption results (not shown), the first optical transition involving excited electronic states in these nanocrystals is located at ~ 2.254 eV, which is nearly 100 meV higher than the XX feature. On the basis of these considerations, the band XX can be assigned to emission from a biexciton, which comprises two lowest-energy excitons.

The fact that the biexciton emission occurs at higher energies than the single-exciton photoluminescence indicates the repulsive character of the X–X interaction, as predicted by our modelling. Further, on the basis of the measured spectral positions of bands X and XX, we obtain $\Delta_{XX} = 106$ meV, which is in good agreement with the value of 91 meV calculated for nanocrystals with the geometrical parameters studied here. Strong X–X repulsion ($\Delta_{XX} > 100$ meV) is consistently observed for type-II CdS/ZnSe nanocrystal samples with different emission colours, as illustrated in the two insets of Fig. 2e. We also detect large X–X interaction energies (~ 80 meV) for type-II nanocrystals of a different composition (ZnTe(core)/CdSe(shell)) with emission in the near-infrared (770 nm). All of these observations point towards the generality of giant X–X repulsion energies in strongly confined type-II colloidal nanoparticles.

Single-exciton optical gain and ASE

To analyse light amplification in type-II CdS/ZnSe nanocrystals, we compare their optical-gain properties with those of traditional type-I CdSe nanocrystals with matching emission wavelengths (Fig. 5). For the biexcitonic gain mechanism operating in type-I nanocrystals, a sharp peak of amplified spontaneous emission (ASE) is red-shifted with respect to the single-exciton band^{6,19} (Fig. 5a, upper spectrum) because of X–X attraction, which decreases the emission energy of biexcitons compared to that of single excitons. For type-II samples, we observe that as we increase the pump level a new, sharp emission feature develops near the position of the single-exciton band (2.01 eV) (Fig. 5b, and the lower spectrum in Fig. 5a). This new peak shows a clear excitation threshold of ~ 2 mJ cm⁻² and a fast, super-linear growth with increasing pump fluence (Fig. 5b, c). The development of a similar sharp feature is also detected using a fixed pump fluence and increasing the size of the excitation spot (variable-stripe-length configuration²⁰). These behaviours are consistent with the ASE regime. An important observation is that the ASE peak develops near the centre of band X, indicating that it is due to stimulated emission of single excitons. This assignment is further confirmed by the observation of a second ASE feature at higher fluences (excitation threshold of ~ 6 mJ cm⁻²), which develops near the position of the high-energy XX band and is due to the traditional biexcitonic gain mechanism (Fig. 5b and c). Similar trends are observed for type-II nanocrystals with other emission wavelengths. For example, for a sample emitting at ~ 2.21 eV, we first detect the emergence of a single-exciton ASE feature, which is followed by the development of a bluer biexcitonic ASE band at ~ 2.36 eV at higher pump fluences.

To further verify the single-exciton character of light amplification in type-II nanocrystals, we perform direct measurements of optical gain using a transient absorption experiment. In these measurements, the absorption change ($\Delta\alpha$) induced in a sample by a short, 100-fs pulse is monitored using a broadband pulse of a femtosecond white-light continuum²¹. The transition to optical gain corresponds

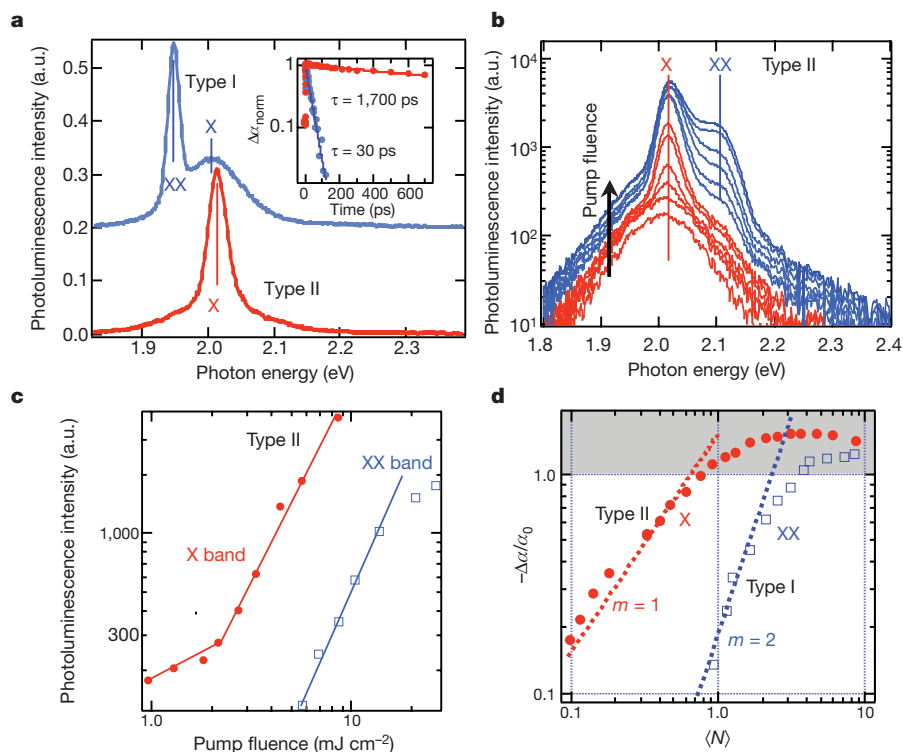


Figure 5 | Optical amplification in type-I and type-II NCs. **a**, Room-temperature ASE spectra of type-I CdSe NCs (blue line; offset vertically for clarity) and type-II CdS/ZnSe NCs (red line; sample is similar to the one shown in Fig. 4) prepared in the form of close-packed drop-cast films and excited by 100-fs pulses at 3 eV. Inset, transient-absorption dynamics measured for these NCs (colour-matched symbols) at the position of the ASE band for the pump intensity that corresponds to the optical-gain onset. **b**, The pump-intensity-dependent photoluminescence spectra of the type-II sample show the development of a narrow ASE peak near the centre of the

single-exciton emission band. The second ASE band, which develops at higher fluences, is located near the XX photoluminescence feature. **c**, Both ASE features show superlinear pump dependence above the threshold pump intensities of $\sim 2 \text{ mJ cm}^{-2}$ (band X) and $\sim 6 \text{ mJ cm}^{-2}$ (band XX). **d**, The dependence of normalized absorption bleaching at the position of the ASE band in type-I (squares) and type-II (circles) NCs (measured $\sim 3 \text{ ps}$ after excitation) as a function of $\langle N \rangle$ in comparison with linear (red straight line) and quadratic (blue straight line) growth. The area shown in grey corresponds to optical gain ($-\Delta\alpha/\alpha_0 > 1$).

to the situation for which absorption bleaching ($\Delta\alpha < 0$) becomes greater than absorption of an unexcited sample (α_0). Figure 5d shows the dependence of the normalized absorption bleaching ($-\Delta\alpha/\alpha_0$) on the average number of excitons per nanocrystal for type-I (squares) and type-II (circles) nanocrystals. In addition to a lower gain threshold (factor of ~ 5 difference), type-II structures clearly show a different functional dependence in the development of the optical gain. In the type-II sample, the initial growth of $|\Delta\alpha|$ is nearly linear (straight red line), whereas in the type-I nanocrystals it is close to quadratic (straight blue line). These observations are consistent with single-exciton (type II) and biexciton (type I) mechanisms of optical gain in these two types of nanostructures.

The single-exciton-gain regime demonstrated here should significantly simplify real-life applications of chemically synthesized nanocrystals in lasing technologies, and specifically should allow realization of nanocrystal lasing under continuous-wave (c.w.) excitation. The pump intensity threshold for producing c.w. gain is approximately determined by the ratio of the threshold fluence measured using ultrafast excitation (see, for example, Fig. 5c) and the gain lifetime²². Because of Auger recombination, this lifetime is in the sub-100 ps range for the multiexcitonic gain mechanism, which leads to very high c.w. lasing thresholds that are well above the nanocrystal-photostability limit. For single-exciton gain, the intrinsic gain dynamics is determined by the radiative single-exciton lifetime, which is typically orders of magnitude longer than the Auger-decay time constants. The difference in relaxation behaviour for single- and biexciton gain mechanisms is illustrated in the inset of Fig. 5a, which shows relaxation dynamics of $\Delta\alpha$ measured at the onset of optical gain for type-I (blue circles) and type-II (red circles) samples. In type-I nanocrystals the measured decay time is 30 ps,

whereas it is more than 50 times longer (1,700 ps) for the type-II nanocrystals.

The present work represents the first practical demonstration of nanocrystal structures that produce optical amplification due to stimulated emission of single-exciton states, which eliminates complications associated with ultrafast multiexciton Auger recombination. This new approach makes use of dynamic splitting of the degeneracy of the lowest-energy emitting transition by giant X–X interactions that develop in type-II heterostructures following spatial separation of electrons and holes. Implementation of the single-exciton gain regime could allow reduction of the lasing threshold under c.w. excitation by orders of magnitude, which could significantly enhance the technological potential of colloidal nanocrystals as ‘soft’, chemically processable optical-gain media.

Received 12 December 2006; accepted 12 April 2007.

1. Alivisatos, A. P. Semiconductor clusters, nanocrystals, and quantum dots. *Science* **271**, 933–937 (1996).
2. Klimov, V. I. (ed.) *Semiconductor and Metal Nanocrystals: Synthesis and Electronic and Optical Properties* (Marcel Dekker, New York, 2003).
3. Murray, C. B., Norris, D. J. & Bawendi, M. G. Synthesis and characterization of nearly monodisperse CdE (E = S, Se, Te) semiconductor nanocrystallites. *J. Am. Chem. Soc.* **115**, 8706–8715 (1993).
4. Eisler, H.-J. *et al.* Color-selective semiconductor nanocrystal laser. *Appl. Phys. Lett.* **80**, 4614–4616 (2002).
5. Malko, A. V. *et al.* From amplified spontaneous emission to microring lasing using nanocrystal quantum dot solids. *Appl. Phys. Lett.* **81**, 1303–1305 (2002).
6. Klimov, V. I. *et al.* Optical gain and stimulated emission in nanocrystal quantum dots. *Science* **290**, 314–317 (2000).
7. Klimov, V. I., Mikhailovsky, A. A., McBranch, D. W., Leatherdale, C. A. & Bawendi, M. G. Quantization of multiparticle Auger rates in semiconductor quantum dots. *Science* **287**, 1011–1013 (2000).

8. Kazes, M., Lewis, D. Y., Evenstein, Y., Mokari, T. & Banin, U. Lasing from semiconductor quantum rods in a cylindrical microcavity. *Adv. Mater.* **14**, 317–321 (2002).
9. Htoon, H., Hollingsworth, J. A., Dickerson, R. & Klimov, V. I. Zero- to one-dimensional transition and Auger recombination in semiconductor quantum rods. *Phys. Rev. Lett.* **91**, 227401 (2003).
10. Ivanov, S. A. *et al.* Light amplification using inverted core/shell nanocrystals: Towards lasing in the single-exciton regime. *J. Phys. Chem. B* **108**, 10625–10630 (2004).
11. Nanda, J. *et al.* Absorption cross sections and Auger recombination lifetimes in inverted core/shell nanocrystals: Implications for lasing performance. *J. Appl. Phys.* **99**, 034309 (2006).
12. Norris, D. J., Sacra, A., Murray, C. B. & Bawendi, M. G. Measurement of the size-dependent hole spectrum in CdSe quantum dots. *Phys. Rev. Lett.* **72**, 2612–2615 (1994).
13. Klimov, V. I. Optical nonlinearities and ultrafast carrier dynamics in semiconductor nanocrystals. *J. Phys. Chem. B* **104**, 6112–6123 (2000).
14. Kang, K. I. *et al.* Confinement-enhanced biexciton binding energy in semiconductor quantum dots. *Phys. Rev. B* **48**, 15449–15452 (1993).
15. Achermann, M., Hollingsworth, J. A. & Klimov, V. I. Multiexcitons confined within a subexcitonic volume: Spectroscopic and dynamical signatures of neutral and charged biexcitons in ultrasmall semiconductor nanocrystals. *Phys. Rev. B* **68**, 245302 (2003).
16. Piryatinski, A., Ivanov, S. A., Tretiak, S. & Klimov, V. I. Effect of quantum and dielectric confinement on the exciton-exciton interaction energy in type-II core/shell semiconductor nanocrystals. *Nano Lett.* **7**, 108–115 (2007).
17. Cao, Y. C. & Wang, J. H. One-pot synthesis of high-quality zinc-blende CdS nanocrystals. *J. Am. Chem. Soc.* **126**, 14336–14337 (2004).
18. Efros, A. L. & Rodina, A. V. Confined excitons, trions, and biexcitons in semiconductor microcrystals. *Solid State Commun.* **72**, 645–649 (1989).
19. Schaller, R. D., Petruska, M. A. & Klimov, V. I. Tunable near-infrared optical gain and amplified spontaneous emission using PbSe nanocrystals. *J. Phys. Chem. B* **107**, 13765–13768 (2003).
20. Shaklee, K. L., Nahory, R. E. & Leheny, R. F. Optical gain in semiconductors. *J. Lumin.* **7**, 284–309 (1973).
21. Klimov, V. I. & McBranch, D. W. Femtosecond high-sensitivity, chirp-free transient absorption spectroscopy using kilohertz lasers. *Opt. Lett.* **23**, 277–279 (1998).
22. Mikhailovsky, A. A., Malko, A. V., Hollingsworth, J. A., Bawendi, M. G. & Klimov, V. I. Multiparticle interactions and stimulated emission in chemically synthesized quantum dots. *Appl. Phys. Lett.* **80**, 2380–2382 (2002).

Supplementary Information is linked to the online version of the paper at www.nature.com/nature.

Acknowledgements This work was supported by the Chemical Sciences, Biosciences and Geosciences Division of the Office of Basic Energy Sciences, US Department of Energy (DOE), Los Alamos LDRD funds, and the Center for Integrated Nanotechnologies jointly operated for DOE by Los Alamos and Sandia National Laboratories.

Author Information Reprints and permissions information is available at www.nature.com/reprints. The authors declare no competing financial interests. Correspondence and requests for materials should be addressed to V.I.K. (klimov@lanl.gov).